International Journal of Gas Turbine, Propulsion and Power Systems
October 2012, Volume 4, Number 3

Non-equilibrium Condensing Flow Modeling in Nozzle and Turbine Cascade

Xiaofeng Zhu[1], Zhirong Lin[1] and Xin Yuan[1]
Tomohiro Tejima[2], Yoshiki Niizeki[2], Naoki Shibukawa[2]

[1] Key Laboratory for Thermal Science and Power Engineering of Ministry of Education
Tsinghua University, BeiJing 100084, P.R. China
sxf03@mails.tsinghua.edu.cn
[2] Toshiba Corporation Power Systems Company, Yokohama 230-0045, Japan

ABSTRACT

This paper presents the development of numerical methods for modeling non-equilibrium condensing flows in steam turbines.

The method is within Eulerian-Eulerian Framework. A Roe convective flux is derived, which is featured on using real steam property and fully coupling wetness fraction with other conservative variables in the Jacobian matrix. The analytical expressions of eigenvalue, right and left side eigenvectors are derived. The real steam property treatment is enlightened by the two-dimensional TTSE method, and the current paper extended it to three dimensions which exhibits great convenience for Eulerian-Eulerian Framework.

Quadrature Method of Moments (QMOM) is implemented to model polydisperse droplet spectrum. To overcome instable issues caused by moment corruption, which is inevitable during steady state time marching, a correction scheme for moments is applied.

Example calculations on nozzles and a turbine cascade are provided. Results show that the current model is robust and correct. QMOM is capable of representing the polydisperse droplet spectrum. Correction schemes play a crucial role for the stability and accuracy of QMOM.

Key words: non-equilibrium; condensing; wet steam; Roe; TTSE; QMOM

INTRODUCTION

A low dissipative convective flux is important for an upwind unstructured condensing solver. Several authors [1,2] have derived the Roe flux for condensing flow under ideal gas and incompressible liquid assumption, which has the same form as the classic single phase flux. Strictly speaking, for multi-phase flow this flux does not theoretically guarantee the RH jump condition, however numerical tests show that the inconsistency is very small when the difference between left and right sides is not too large. The Roe type flux that strictly satisfies the jump condition could be derived by elaborate construction, but is not unique [3].

Real steam property is crucial for condensing flow simulation, because nucleation and droplet growth rate are sensitive to properties such water/vapor density, specific heat ratio, evaporation enthalpy, etc. Generally, there are two classes of methods handling real steam property. One is to use an equation of state with empirical correction of the compressibility coefficient [4] or use the more complex virial equation [5], and properties such as enthalpy, specific heat are derived by differentiate or integral the EOS. The other class is to construct a steam table, and properties are got by linear interpolation. A more elegant way is to use Tabular Taylor Series Expansion method (TTSE), where accurate first order derivatives are pre-computed and stored, and are used for calculating second order derivatives when doing interpolation [6]. The original TTSE method takes steam density and internal energy as independent variables, which is natural for Eulerian-Lagrangian framework, but inconvenient for Eulerian-Eulerian framework where the mixture density, internal energy, and wetness fraction are used as degrees of freedom. The current paper extended TTSE method to directly use these three variables. Much work was done in order to derive analytical first order partial derivatives of p, T to mixture density, internal energy and wetness.

For condensing flow, an aspect of particular importance is the modeling of polydisperse droplet spectrum. Commercial software such as Fluent can only deal with monodisperse droplet. The Method of Moments (MOM) was applied in order to modeling the polydisperse droplet size distribution [7]. This method exhibits comparable accuracy with the benchmark Eulerian-Lagrangian method [8]. In conventional MOM, the droplet growth law of the non-equilibrium condensing theory cannot be handled directly without linear approximation. To solve this problem, the QMOM method was first introduced by McGraw [9], where Gaussian quadrature was used for the integral terms related to growth law, and abscissas and weights were obtained from the moments set. Recently, this method was successfully applied to condensing steam flow by Gerber [10], and results show that the method is able to represent polydisperse droplet spectrum, though no evident advantage was shown over MOM, probably because the condensing phenomena in nozzles is relatively simple and polydispersion is not notable.

The implementation of QMOM method for steady state problem encounters more difficulty than the original method for the ordinary differential problem [11]. The inverse problem that gets abscissas and weights from the moments set highly depends on the validity of moments data. During early stages of a time marching scheme, it is quite normal that the flow field may be disturbed and moments data could be corrupt, so without a correction scheme the time marching may not converge and even diverge. To cure this problem, Petitti [11] proposed a correction algorithm based on work by McGraw [12] and Wright [13]. However, this method is not theoretically adequate for moments set of six, because it misses checking the 3×3 determinants in the moments set which does not fully conform to the original McGraw's method. In the current implementation, Petitti's method is adopted, with an addition of 3×3 determinants checking.

GOVERNING EQUATIONS

Main Governing Equations for Two Phase Flow

Phase slip is not considered here. The governing equations for two phase flow are given in the following PDE form

Presented at International Gas Turbine Congress 2011 Osaka, November 13-18, Osaka, Japan, IGTC2011-0104
Review completed July 31, 2012

$$\partial_t W + \partial_x F + \partial_y G = S \tag{1}$$

Where

$$\begin{aligned} W &= [\rho, \rho u, \rho v, \rho E, \rho\beta] \\ F &= [\rho u, \rho u^2 + p, \rho uv, \rho uH, \rho u\beta] \\ G &= [\rho v, \rho uv, \rho vv + p, \rho vH, \rho v\beta] \\ S &= [0, 0, 0, 0, S_\beta] \end{aligned} \tag{2}$$

Where ρ is density, E is total internal energy and β is the wetness.

If the vapor phase behaves as ideal gas, the above equations can be closed by the following pressure equation [1]

$$p = (\gamma - 1)\frac{1-\beta}{1+\beta(\gamma-1)}\left[\rho E - \frac{1}{2}\rho(u^2+v^2) + \rho\beta L\right] \tag{3}$$

Where L is the enthalpy of evaporation, and γ is the specific heat.

When accuracy is needed, a real steam property should be used, and then p usually becomes an implicit function of ρ, e, and β.

Droplet Distribution Transportation Equations

Two basic parameters of non-equilibrium condensing theory are droplets number and their radius. The evolution of droplets depends on environmental pressure, temperature, and each single droplet's radius and thermal property. If droplet spectrum is modeled as monodisperse, only one additional transportation equation of droplet number is needed, comparing with equilibrium governing equations. If MOM method is used to model polydispersion, the number of additional equations is equal to be number of moments minus 1. The only differences between QMOM and the conventional MOM are the number of moments used and how these moment transportation equations are closed. MOM's transportation equations are listed as following (these equations are solved together with main governing equations)

$$\begin{aligned} W &= [\rho, \rho u, \rho v, \rho E, \rho\beta, \rho Q_0, \rho Q_1, \rho Q_2] \\ F &= [\rho u, \rho u^2 + p, \rho uv, \rho uH, \rho u\beta, \rho uQ_0, \rho uQ_1, \rho uQ_2] \\ G &= [\rho v, \rho vu, \rho vv + p, \rho vH, \rho v\beta, \rho vQ_0, \rho vQ_1, \rho vQ_2] \\ S &= [0, 0, 0, 0, S_3, S_0, S_1, S_2] \end{aligned} \tag{4}$$

Where

$$\begin{aligned} S_3 &= \left(3\rho\int r^2 g(r) f(r) dr + Jr_*^3\right)\frac{4}{3}\pi\rho_l \\ S_2 &= 2\rho\int r g(r) f(r) dr + Jr_*^2 \\ S_1 &= \rho\int g(r) f(r) dr + Jr_* \\ S_0 &= J \end{aligned} \tag{5}$$

Where $g(r)$ is droplet growth raw, J is nucleate rate per unit volume, $f(r)$ is the distribution of droplet radius (number of droplets per unit length of radius and per unit mass of mixture), and Q_i is the i-th moment, defined as

$$Q_k = \int r^k f(r) dr \tag{6}$$

The wetness β has a direct relation with Q_3

$$\beta = \frac{4}{3}\pi\rho_l Q_3 \tag{7}$$

In MOM method, eq. (5) has to be close by approximating growth law to the form

$$g(r) = a_1 + a_2 r \tag{8}$$

Most papers further simplify eq. (8) by

$$g(r) = \sqrt{Q_2 / Q_0} \tag{9}$$

Upwind Flux Using Real Steam Property

The Roe flux employed here is an extension of that proposed by Mei [1] and also Halama [2], which only deals with ideal steam. The key point of current work is to derive the Jacobian without any assumption of the equation of state of the vapor/water mixture. Results are listed here.

The Two phase Roe flux has the same form as the single phase one

$$F(W_L, W_R) = \frac{1}{2}\left(F_L + F_R - E\left|\Lambda\right|E^{-1}(W_R - W_L)\right) \tag{10}$$

Where

$$\Lambda = \mathrm{diag}(u - \hat{a}, u, u, u, u + \hat{a}, u, u, u) \tag{11}$$

$$E = \begin{bmatrix} 1 & 0 & 1 & 1 & 1 & 0 & 0 & 0 \\ u-\hat{a} & 0 & u & u & u+\hat{a} & 0 & 0 & 0 \\ v & 1 & v & v & v & 0 & 0 & 0 \\ H - u\hat{a} & v & \alpha_1 & \alpha_2 & H + u\hat{a} & 0 & 0 & 0 \\ \beta & 0 & \beta & 1 & \beta & 0 & 0 & 0 \\ Q_2 & 0 & 0 & 0 & Q_2 & 1 & 0 & 0 \\ Q_1 & 0 & 0 & 0 & Q_1 & 0 & 1 & 0 \\ Q_0 & 0 & 0 & 0 & Q_0 & 0 & 0 & 1 \end{bmatrix} \tag{12}$$

$$\begin{aligned} \hat{a}^2 &= -\left(u^2\frac{\partial p}{\partial w_3} - v\frac{\partial p}{\partial w_2} - \beta\frac{\partial p}{\partial w_4} - H\frac{\partial p}{\partial w_3} - \frac{\partial p}{\partial w_0}\right) \\ &= \frac{\partial p}{\partial \rho} + \frac{p}{\rho^2}\frac{\partial p}{\partial e} \end{aligned} \tag{13}$$

$$\alpha_1 = H - \left(\frac{\partial p}{\partial w_3}\right)^{-1}\hat{a}^2 \tag{14}$$

$$\alpha_2 = H - \left(\frac{\partial p}{\partial w_3}\right)^{-1}\left(\hat{a}^2 + (1-\beta)\frac{\partial p}{\partial w_4}\right) \tag{15}$$

Where w_i is i-th conservative variable.

The pressure derivatives to conservative variables could be expressed in terms of derivatives to mixture density, internal energy, and wetness, which can be calculated either by solving real vapor/water equations or by interpolating a steam stable. When ideal steam equation is used, eq. (11)-(14) reduce to the same expressions as in previous work [1, 2]. The inverse of matrix E can be calculated either analytically (as given in Appendix A) or numerically. If numerical inverse is used, care should be taken that matrix E is ill-conditioned, thus should be treated as a block lower triangular matrix, and numerical inverse is performed only on the well-conditioned 5 by 5 sub-matrix.

IMPLEMENTAION OF QMOM METHOD

Theory and Implementation

Like MOM, QMOM method is devised to calculate the integral terms in eq. (5). The number of moments in QMOM is an even number, i.e. 2, 4, 6, or higher. 6 is a common choice, and higher order moments are not encouraged to use, because it is not computational efficient and inclined to cause numerical instability. This paper only focuses on QMOM with 6 moments. The conservative variables for QMOM are:

$$W=[\rho,\rho u,\rho v,\rho E,\rho\beta,\rho Q_0,\rho Q_1,\rho Q_2,\rho Q_4,\rho Q_5] \quad (16)$$

Source terms for ρQ_0~ρQ_2 and $\rho\beta$ are the same as for eq. (5), and source terms of ρQ_4 and ρQ_5 are

$$\begin{aligned} S_4 &= 4\rho\int r^3 g(r) f(r)dr + Jr_*^4 \\ S_5 &= 5\rho\int r^4 g(r) f(r)dr + Jr_*^5 \end{aligned} \quad (17)$$

Subheadings are underlined, typed with the initial letter of each word capitalized, and placed flush left. One line of space is left above the subheading, and the text begins on the next line below it.

The integrals in eq. (5) and (17) are calculated by the Gaussian quadrature law

$$\int r^j g(r) f(r)dr = \sum_{i=0}^{n} r_i^j g(r_i) w_i \quad (18)$$

Where $f(r)$ is regarded as the weight function. The form of growth law is no longer constrained. r_i and w_i are calculated from the moments Q_0~Q_5 according to the Gaussian quadrature law

$$\sum_{i=0}^{3} r_i^j w_i = \int r^j f(r)dr = Q_j, \text{for j=0~5} \quad (19)$$

Eq. (19) can be efficiently solved by product difference algorithm described by McGraw [9].

It is worthy to point out that eq. (18) is not accurate theoretically. After all, Gaussian quadrature implies that the accuracy of eq. (18) is guaranteed only when $r^j g(r)$ is a polynomial of order less than 5. As the maximum j is 4, $g(r)$ has to be a linear function to guarantee accuracy. Therefore, QMOM deals with integrals in source terms by sacrificing integrals' accuracy, while MOM handles this by approximating droplet growth law.

Moreover, when the droplet spectrum is near monodispersion, one of r_i in eq. (18) may become much smaller than the critical radius, thus make $g(r_i)$ near negative infinity, and make the liquid phase evaporate at one time step. This phenomenon is obviously non-physical, and can cause numerical instability. A cure for this problem is to limit $r_i^j g(r_i) w_i$ to be not smaller than a const negative ratio of the moment which represents:

$$r_i^j g(r_i) w_i = \max(r_i^j g(r_i) w_i, -2 r_i^{j+1} w_i) \quad (20)$$

Correction algorithm

During time marching, especially at early steps, moments series may not be valid (i.e. corrupted), thus make it impossible to get correct abscissas and weights. Even after the solution is converged, it has not been proved that every solution point has valid moments. Moreover, physically not all regions are suitable for QMOM. For example, when following the steam's track in a divergent nozzle with superheated vapor inlet, moments are zero initially, then monodisperse (as droplet growth rate is very low at first), and at last polydisperse. It is obvious that product difference algorithm is invalid in zero or monodisperse regions. So, corrections have to be made before doing the product difference algorithm. The current procedures mainly follow Petitti [11], and some necessary adjustments are done to make the algorithm more robust.

The full (necessary and sufficient) condition for a valid moment set is the positivity of the following determinants derived from the moments [12, 14]:

$$\Delta_{n,l} = \begin{vmatrix} m_n & m_{n+1} & \cdots & m_{n+l} \\ m_{n+1} & m_{n+2} & \cdots & m_{n+l+1} \\ \vdots & \vdots & \vdots & \vdots \\ m_{n+l} & m_{n+l+1} & \cdots & m_{n+2l} \end{vmatrix} \geq 0, \text{ for } n=0,\ 1 \text{ and } l \geq 0 \quad (21)$$

A necessary condition for a valid moment set is the convexity requirement:

$$m_k m_{k-2} - m_{k-1}^2 \geq 0 \quad (22)$$

The first part of the correction procedures is to recover corrupted moments to assure the necessary and sufficient condition. The method adopted for recovering invalid moments set is the Minimum Square Algorithm developed originally by McGraw [12] and also described by Petitti [11]; it is an iterative method based on the idea of identifying and correcting only the moment of index k^* which after adjustment maximizes the smoothness of the function $ln(m_k)$, through a minimization procedure. It is worthy to note that: Petitii's implementation did not check all the terms in eq. (21) which is found to be inadequate for current problems, therefore the current paper strictly conform to the original method which not only check the necessary condition eq. (22), but also check the 3 by 3 determinate which together with eq. (22) form the full condition for a six moments set; Different from the original method, here we only adjust m_1,m_2,m_4,m_5, because m_0 and m_3 are directly related to the droplet number and wetness, and adjusting these two value has more physical impact to the flow field thus may causes numerical oscillation or even instability.

Sometimes the above correction may not succeed after an acceptable number of iterations. In case it failed, the second correction procedure is applied [11]. The idea is to restore the corrupted moments with the moments calculated as the arithmetic mean of those two log-normal distributions. The distributions are evaluated from the first four moments, while keeping fixed m_0 and m_3.

The detailed correction procedures are described in Appendix B.

TABLE FOR MIXTURE BY TTSE METHOD

A table for vapor and water mixture is constructed based on the TTSE idea, which is originally devised for single phase property by Hill [6]. The table's shape is actually a cubic, where the independent variables are ρ, e, β. In this table, the vapor' and water's temperature are considered to be the same, however the current method is also applicable to some authors' suggestion [15] that the droplet's temperature should be better treated as the local saturation temperature $T_s(p)$.

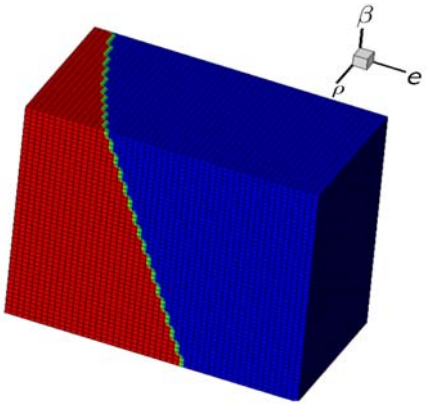

Fig. 1 The TTSE table

As Fig. 1 shows, a 100×100×100 grid is used, where β, e and $ln(\rho)$ are equally spaced. Ranges of ρ, e and β are 0.02~2.0 kg/m^3, 2.0E6~2.9E6 J/kg, 0~10% respectively and the corresponding range of p, T are 0.0012~0.58 MPa and 173.8~634.3K. These parameter ranges cover most low pressure steam turbine conditions. Water in the blue region is overheated, and vapor in the red region is overcooled. Once the table has been set up, any property Φ is calculated as:

$$\phi(\rho,e,\beta)=\phi_{i,j,k}+\frac{\partial\phi}{\partial\rho}\Delta\rho+\frac{\partial\phi}{\partial e}\Delta e+\frac{\partial\phi}{\partial\beta}\Delta\beta+$$
$$\frac{1}{2}\frac{\partial^2\phi}{\partial\rho^2}(\Delta\rho)^2+\frac{1}{2}\frac{\partial^2\phi}{\partial e^2}(\Delta e)^2+\frac{1}{2}\frac{\partial^2\phi}{\partial\beta^2}(\Delta\beta)^2+ \quad (23)$$
$$\frac{\partial^2\phi}{\partial\rho\partial e}\Delta\rho\Delta e+\frac{\partial^2\phi}{\partial\rho\partial\beta}\Delta\rho\Delta\beta+\frac{\partial^2\phi}{\partial e\partial\beta}\Delta e\Delta\beta$$

Where i, j, k are node indexes; Φ and its first order derivatives are previously accurately calculated and stored on nodes. Φ's second order derivatives are calculated numerically by centre difference of the first order derivatives.

The table is constructed from IAPWS97 formulas [20]. As it is more convenient to get derivatives of ρ, e, and β to p, T, and β, first order derivatives of p, T, and β are calculated by the following Jacobian relationship

$$\left[\frac{\partial p,T,\beta}{\partial\rho,e,\beta}\right]\left[\frac{\partial\rho,e,\beta}{\partial p,T,\beta}\right]=I \quad (24)$$

Other derivative for property such as h, Cp are calculated by

$$\left[\frac{\partial\phi}{\partial\rho,e,\beta}\right]=\left[\frac{\partial\phi}{\partial p,T,\beta}\right]\left[\frac{\partial p,T,\beta}{\partial\rho,e,\beta}\right] \quad (25)$$

The pressure interpolation error is shown in Fig. 2. The error is defined as ratio of difference between the accurate and the approximate value to the accurate value. At each wetness level, three pressure error curves are plotted (minimum, mediate, and maximum density levels). In most of regions, errors are readily below 1E-5. The error larger than 1E-4 is caused by the unsmooth transition between Region 2s' basic equation and supplementary equation for the metastable-vapor region in IAPWS97. This error could be reduced if using more consistent formulas such as the unified fundamental equation by Hill [16]. The temperature interpolation error has the similar magnitude, so is not plotted here.

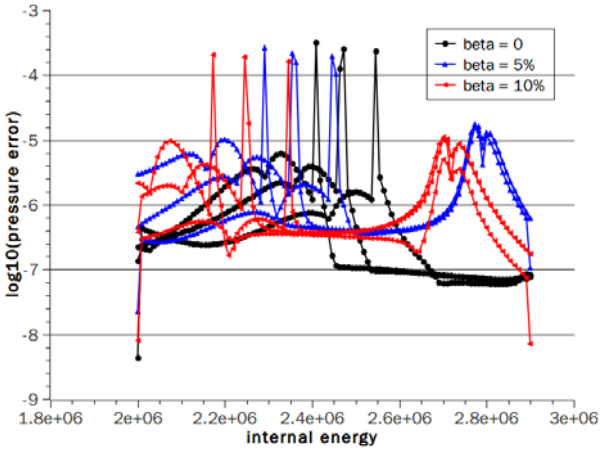

Fig.2 Pressure interpolation error of the TTSE table

NON-EQUILIBRIUM CONDENSING MODEL

Vapor does not condense immediately it expands from superheated state to the saturation line. It becomes water through two ways: directly nucleates into very small droplets, or condenses on existing particles' surface (either on droplets or on minute dirt). Nucleating rate and droplet growth rate nonlinearly depend on pressure, saturation ratio, droplet radius and etc. The detailed homogeneous condensing theory has been reviewed in several literatures [17, 18].

The nucleate law here adopts the classic nucleate rate with the modification by Courney and Kantrowitz (1951) [17, 18]

$$J=\frac{q}{1+\eta}\left(\frac{2\sigma}{\pi m^3}\right)^{1/2}\frac{\rho_s(T_g)}{\rho_l}\exp\left(-\frac{4\pi r_*^2\sigma}{3kT_g}\right) \quad (26)$$

Where η is the modification factor; r^* is critical radius; q is condensing coefficient; foot note l, g represent liquid and gas respectively; ΔT is supercooling temperature; $\rho_s(T_g)$ is density of saturation vapor; h_{fg} is equilibrium latent heat; γ is specific heat ration; σ is surface tension coefficient; R is gas constant; κ is Boltzmann constant; m the molecular mass of water

$$\eta=\frac{2(\gamma-1)}{(\gamma+1)}\frac{h_{fg}}{RT_g}\left(\frac{h_{fg}}{RT_g}-\frac{1}{2}\right) \quad (27)$$

$$r_*=\frac{2\sigma T_s}{\rho_l h_{fg}\Delta T} \quad (28)$$

The growth rate is determined by the energy balance including the latent heat and convective heat transfer between the droplet and the surrounding vapour:

$$\frac{dr}{dt}=\frac{\alpha(T_l-T_g)}{\rho_l(h_g-h_l)} \quad (29)$$

Where α is the heat transfer coefficient. As a droplet can grows larger by several orders, α is not a constant. Also, the liquid temperature T_l has to be modeled. The formula of Gyarmathy [17, 18] is commonly thought to be of considerable accuracy:

$$\alpha=\frac{\lambda_g}{r(1+3.18K_n)} \quad (30)$$

$$T_l=T_s-\Delta T\frac{r_*}{r} \quad (31)$$

Where λ_g is vapor thermal conductivity; K_n is Knudsen number, defined as

$$K_n=l/(2r) \quad (32)$$

Where l is the molecular free path, defined as

$$l=\left(1.5\mu_g\sqrt{RT_g}\right)/p \quad (33)$$

The final expression of growth law is

$$\dot{r}=\frac{1}{\rho_l}\frac{\lambda_g}{(1+3.18K_n)}\frac{r-r^*}{r^2}\frac{T_s-T_g}{h_{fg}} \quad (34)$$

Another frequently-used growth law is also implemented [10, 15]:

$$\dot{r}=\frac{1}{\rho_l}\frac{\lambda_g}{(r+1.89(1-\upsilon)l/\mathrm{Pr})}\frac{r-r^*}{r}\frac{T_s-T_g}{h_{fg}} \quad (35)$$

Where Pr is the Prandtl number of vapor; $(1-\upsilon)$ is a semi-empirical correction, and υ is given in [4]

$$\upsilon=\frac{R_gT_g}{h_{fg}}\left(\alpha-0.5-\frac{2-q_c}{2q_c}\frac{\gamma+1}{2\gamma}\frac{C_{pg}T_s}{h_{fg}}\right) \quad (36)$$

Where α is an empirical parameter, which typically takes values between 0~5.

In following calculations, eq. (34) is referenced as the classic growth law, and eq. (35) is referenced as the Young growth law, with α takes 5.

VALIDATION AND DISCUSSION

The above algorithm is integrated into a second order unstructured cell-centered finite volume Euler solver, where least square method is used for reconstruction and the Venkatakrishnan limiter [19] is used to guarantee the monotonicity principle. Real

steam property is decided automatically according to the steam table and other official physical property formulas [21-23]. Unless otherwise specified, no artificial adjustment is used to get a better agreement with experiment data.

Calculation of Barschdorff Nozzle

The Barschdroff nozzle is an arc nozzle with the critical throat height 60 mm and radius of wall curvature 584 mm. The boundary conditions are: inlet total pressure 0.0785 MPa, total temperature 380.55 K, supersonic outlet. A mesh of 40×300 is created. The droplet growth law uses the classic one. Results are shown in Fig. 3, where centre line pressure is compared with experiment [24] and both pressure and Sauter mean radius is compared with literature [25].

The pressure distribution is close with experiment, and agrees well with Heiler's calculation. The result could be improved if inlet temperature is adjusted round +1 K, considering the experiment's uncertainty. The difference between MOM and QMOM is obvious near the condensation shock. The location of condensation shock predicted by QMOM is a little earlier than MOM, while the Sauter mean radius is underestimated. As Fig. 4 shows, the nucleate rate and droplet number calculated by QMOM is higher than MOM, which explains the earlier condensation shock location. While final wetness is almost the same for both, it is reasonable that the Sauter mean radius predicted by QMOM is lower than that by MOM.

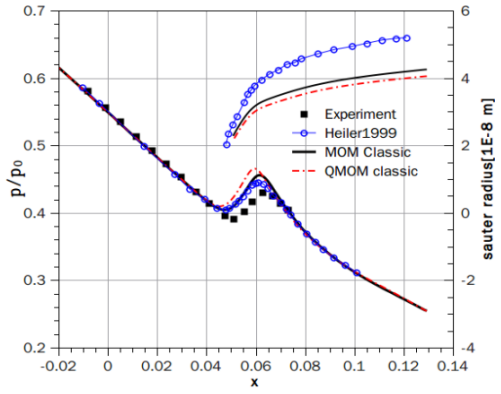

Fig. 3 Comparison of centre line pressure with experiment, and centre line pressure and Sauter mean radius with literature.

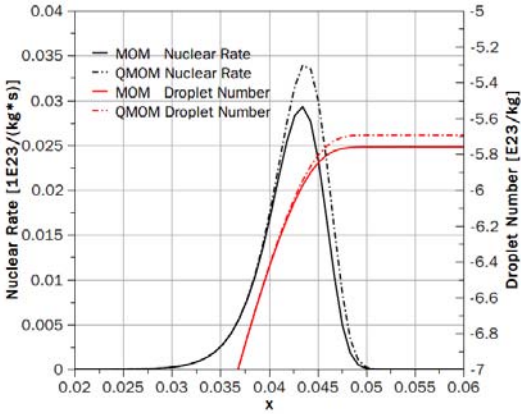

Fig. 4 Centre line nucleate rate and droplet number

Calculation of Moses/Stein Nozzle

The Moses/Stein nozzle [26] case 410 was calculated and compared with experiment to verify the numerical model. A mesh of 40×300 was created for the nozzle geometry. The inlet, outlet, and throat is at x=0.06m, x=0.14m, and x =0.0822m respectively. The boundary conditions are: inlet total pressure 0.070727 MPa, total temperature 377 K, supersonic outlet. Calculations were done with two sets of options: the growth rate by Young and the classic growth rate; MOM and QMOM.

The location of condensation shock agrees fairly well with experiment. However the pressure distribution after the condensation shock displays a departure from the experimental data. Though some calculation in literature [27] also shows this departure, more insight is needed to explain this phenomenon.

One profit of QMOM is that the weights and abscissas of Gaussian quadrature can be directly used to represent the polydisperse droplet distribution. As Fig. 5 shows, at x=0.095, two of the three weights are near zero, which means the distribution before the condensation shock are almost monodisperse; at x=0.105, three weights have the same order of magnitude, indicting the distribution are polydisperse; and at exit, the polydispersion fades a little.

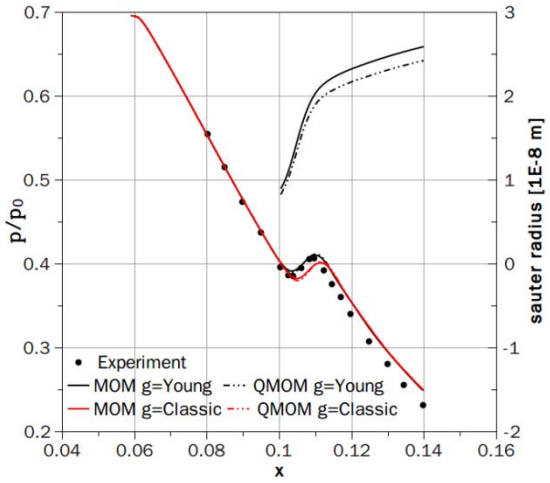

Fig. 5 Centre line pressure and Sauter mean radius. Pressure comparison with experiment

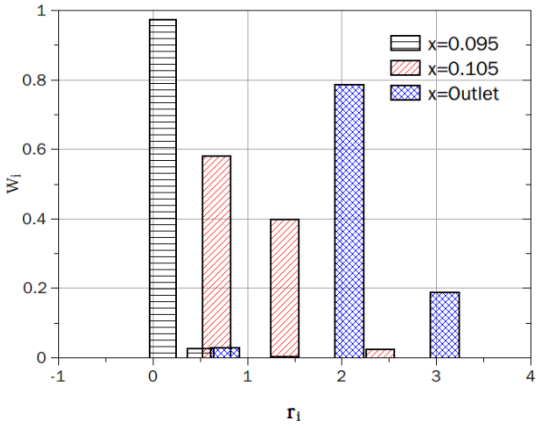

Fig. 6 Centre line droplet spectrum represented by r_i, w_i

Calculation of Bakhatar Cascade

The rotor tip experimental data of Bakhtar et al. [28] was used to test the model in more complex situation. A multi-block mesh with the same topology [5] and similar cell count was made. The inlet total condition is p0=0.0999MPa, T_0=360.82K (i.e. 10K supercooling), and the outlet static pressure is 0.042672MPa.

Two calculations were performed. In the first case, standard physical properties and growth rate of Young are used; in the second case, corrections are applied to the surface tension coefficient and the growth rate, such that $\sigma=1.08\sigma_{std}$, $J=0.6J_{Young}$.

Fig. 7 compares the calculated pressure profile with experiment. On the pressure side, the comparison is good. However, on the suction side, the condensation shock from the first calculation is weaker than experiment, and agreed much better in the second calculation, which is in consistent with other scholar's experience that artificial adjustment is necessary to give agreement with experiment [5, 15].

Fig.8 shows the wetness fraction. The condensation regions of pressure side and suction side actually connect. The overcooling in this region is caused by the expansion fan beginning at suction side's trailing edge. Beside the expansion fan, the large pressure difference between two sides of the trailing edge also causes the shock at suction side. Although the calculation is inviscid, it is common that the large curvature of trailing edge could induce a wake. The wetness fraction reduces through the shock.

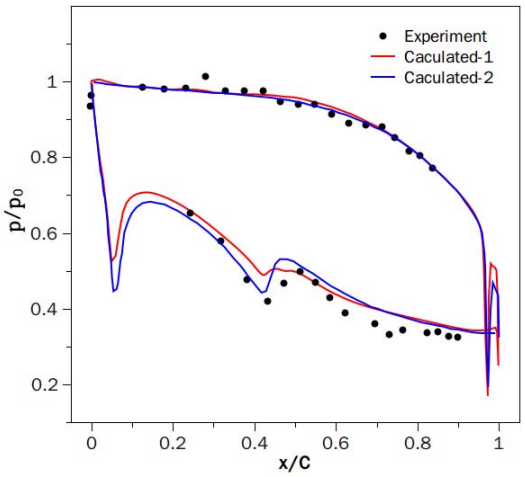

Fig. 7 Comparison of pressure with experiment

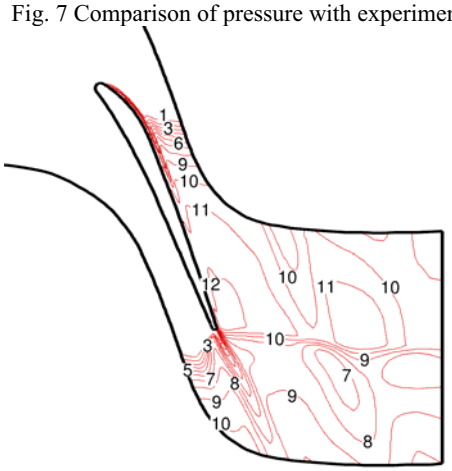

Fig. 8 Calculated wetness fraction distribution (one level represents 0.5%)

CONCLUSION

A multi-phase model is presented for non-equilibrium condensing steam flow under Eulerian-Eulerian framework. A Roe type convective flux is derived, which uses real steam property and fully considers the coupling between wetness fraction and mixture conservative variables. A method that models real steam property by a three-dimensional TTSE table is presented in order to eliminate the difficulty in using two-dimensional single phase steam table under Eulerian-Eulerian framework. This TTSE table could provide adequate accuracy in a wide range of low pressure steam condition.

The Quadrature Method of Moments (QMOM) has no limitation to droplet growth law, and thus can theoretically provide better polydisperse droplet distribution modeling. This method is implemented in the framework. To overcome the data corrupt during steady state time marching, the correction method developed by McGraw et al is adopted and some necessary adjustment is done to make the correction algorithm more robust for condensing steam flow.

The model is verified by two nozzle and one cascade cases calculation and comparison with experimental data. Generally, the nozzle pressure comparison is good and is in accord with some classic literature. The Sauter radius strongly depends on droplet number and the shape of droplet radius distribution, thus is more difficult to predict, and the differences between results by current methods and literature is apparent. The effect of QMOM to flow field is mainly at regions near condensation shock. Though theoretically more advantage, from current calculation it is hard to tell whether QMOM method provided better results than MOM, partly because that the droplet growth law and the nucleate law dominate the multi-phase model and their uncertainties should have more impact on results.

ACKNOWLEDGEMENT

This study is supported by Tsinghua-Toshiba Energy & Environment Research Center, the National Natural Science Foundation of China (Grant No. 50676043) and the Special Funds for Major State Basic Research Projects (Grant No. 2007CB210108).

References

[1] Mei, Y., and Guha, A., 2006,Modification of the upwind schemes for the computation of condensing two-phase flows. Pro. IMechE Vol. 220 Part A: J. Power and Energy, pp. 809-814

[2] Halama, J., Benkhaldoun, F., and Fort, J., 2010, Flux schemes base finite volume method for internal transonic flow with condensation, Int. J. Numer. Meth. Fluids, DOI: 10.1002/fld.2223,

[3] Mottura, L., Vigevano, L., and Zaccanti, M., An evaluation of Roe's scheme generalization for equilibrium real gas flows, Journal of Computational Physics, Vol. 138, pp.354-399.

[4] Young, J. B., 1992, Two-dimensional nonequilibrium wet-steam calculations for nozzles and turbine cascades, Journal of Turbomachinery, Vol. 114, pp. 569-579.

[5] Gerber, A. G., and Kermani, M. J., 2004, A pressure based Eulerian-Eulerian multi-phase model for non-equilibrium condensation in transonic steam flow, Int. J. Heat Mass Transfer, Vol. 47, pp. 2217-2231

[6] P. G. Hill, K. Miyagawa, J. D. Denton, Fast and accurate inclusion of steam properties in two- and three-dimensional steam turbine flow calculations. Proc. Inst. Mech. Eng. 214 (Part C), 903-919, 2000.

[7] Hill, P.G. Condensing of water vapour during supersonic expansion nozzles. J. Fluid Mech. 1966(25), 593-620

[8] White, A. J., 2003, A comparison of modelling methods for polydispersed wet-steam flow, Int. J. Numer. Meth. Engng, Vol. 57, pp.819-834

[9] R. McGraw, Description of aerosol dynamics by the quadrature method of moments, Aerosol Science and Technology, 1997, Vol. 27, No. 2, 255-265

[10] Gerber, A. G., and Mousavi, A., 2007, Representing polydispersed droplet behavior in nucleating steam flow, Journal of Fluids Engineering, Vol. 129, pp. 1404-1414.

[11] M. Petitti, A. Nasuti, etc. Bubble size distribution modeling in stirred gas-liquid reactors with QMOM augmented by a new correction algorithm. AICheE Journal, 2010, Vol. 56, No. 1, 36-53

[12] R. McGraw, Correcting moment sequences for errors associated with advective transport, 2006, Available at: http://www.ecd.bnl.gov/pubs/momentcorrection_mcgraw2006.pdf

[13] D. L. Wright Jr, Numerical advection of moments of the particle size distribution in eulerian models. J Aerosol Sci., 2007(38), 352-369

[14] Shohat, J. A., and Tamarkin, J. D., 1950(Revised edition), The problem of moments, American Mathematical Society, New York.

[15] Simpson, D. A., and White, A. J., 2006, Viscous and unsteady flow calculations of condensing steam in nozzles, Int. J. Heat and Fluid Flows, Vol. 26, pp. 71-79.

[16] P. G. Hill, A unified fundamental equation for the

thermodynamic properties H2O, J. Phys. Chem. Ref. Data, Vol. 19, No. 5, 1990, 1233-1274.
[17] Bakhtar, F., Young, J. B., White, A. J, and Simpson, D. A., 2005, Classical nucleation theory and its application to condensing steam flow calculations. In Proc. Inst. Mech. Eng., Part C: J. Mech. Eng. Sci., Vol. 219, pp. 1315-1333.
[18] Bakhtar, F., White, A. J., and Mashmoushy, H., 2005, Theoretical treatments of two-dimensional two-phase flows of steam and comparison with cascade measurements. In Proc. Inst. Mech. Eng, Part C: J. Mech. Eng. Sci., Vol. 219, pp. 1335-1355.
[19]Venkatakrishnan, V., 1993, 31st Aerospace Sciences Meeting & Exhibit. AIAA Paper 93-0880
[20] IAPWS, 2007, IAPWS release on the IAPWS industrial formulation 1997 for the thermodynamic properties of water and steam, IAPWS Meeting at Lucerne, Switzerland.
[21] IAPWS, 1994, IAPWS release on surface tension of ordinary water substance, IAPWS Meeting at Orlando, USA.
[22] IAPWS, 2008, Revised release on the IAPS formulation for the thermal conductivity of ordinary water substance, IAPWS Meeting at Berlin, Germany.
[23] IAPWS, 2008, Revised release on the IAPWS formulation 2008 for the viscosity of ordinary water substance, IAPWS Meeting at Berlin, Germany.
[24] Barschdorff, D., 1971, Verlauf der zustandsgrössen und gas-dynamische zusammenhänge bei der spontanen kondensation reinen Wasserdampfes in Lavaldüsen. Forschung im Ingenieurwesen, 37 (5), pp. 146-157.
[25] Heiler, M., 1999, Instationäre phänomene in homogen/heterogen kondensierenden düsen-und Turbinenströmungen, Dissertation, Fakultät für Maschinenbau, Universität Karlsruhe, Germany.
[26] Moses, C. A., and Stein, G. D., 1978, On the growth of steam droplets formed in a laval nozzle using both static pressure and light Scattering Measurements, Journal of Fluids Engineering, Vol. 100, pp. 311-322.
[27] Zori, L., and Kelecy, F., 2005, Wet steam flow modeling in a general CFD Flow Solver, 35th AIAA Fluid Dynamics Conference and Exhibit, AIAA 2005-5276
[28] Bakhtar, F., Ebrahimi, M., and Webb, R. A., 1995, On the performance of a cascade of turbine rotor tip section blading in nucleating steam. Part 1: Surface Pressure Distributions, Proc. Inst. Mech. Eng., Part C: J. Mech. Eng. Sci., Vol. 209, pp. 115-124

Appendix A

Lets rewrite E of eq. (12) in the form of block lower triangle matrix

$$E=\begin{bmatrix} A & 0 \\ B & I \end{bmatrix} \tag{A.1}$$

Where A is a 5 by 5 matrix, E's inversion is given by

$$E^{-1}=\begin{bmatrix} A^{-1} & 0 \\ -BA^{-1} & I \end{bmatrix} \tag{A.2}$$

A can be inversed analytically by solve $AA^{-1}=I$, which leads to a linear equations for each row vector A. A^{-1} is given by

$$\begin{bmatrix} a_{00} & \dfrac{-1}{2\hat{a}}-ua_{03} & -va_{03} & \dfrac{1}{2(H-\alpha_1)} & \dfrac{-(\alpha_2-\alpha_1)}{1-\beta}a_{03} \\ -v & 0 & 1 & 0 & 0 \\ a_{20} & -ua_{23} & -va_{23} & \dfrac{1}{\alpha_1-H} & \dfrac{-1-(\alpha_2-\alpha_1)a_{23}}{1-\beta} \\ \dfrac{-\beta}{1-\beta} & 0 & 0 & 0 & \dfrac{1}{1-\beta} \\ a_{40} & \dfrac{-1}{2\hat{a}}-ua_{43} & -va_{43} & \dfrac{1}{2(H-\alpha_1)} & \dfrac{-(\alpha_2-\alpha_1)}{1-\beta}a_{43} \end{bmatrix} \tag{A.3}$$

Where

$$\begin{aligned} a_{00} &= -\left[\alpha_1-u^2-v^2-\frac{\beta}{1-\beta}(\alpha_2-\alpha_1)\right]a_{03}+\frac{u}{2\hat{a}} \\ a_{20} &= -\left[H-u^2-v^2-\frac{\beta}{1-\beta}(\alpha_2-\alpha_1)\right]a_{23}+\frac{\beta}{1-\beta} \\ a_{40} &= -\left[\alpha_1-u^2-v^2-\frac{\beta}{1-\beta}(\alpha_2-\alpha_1)\right]a_{43}-\frac{u}{2\hat{a}} \end{aligned} \tag{A.4}$$

Appendix B

Before going into algorithm details, it is useful to introduce the difference table of the function $ln(m_k)$. As shown in Table B.1 and Table B.2, items in each column are got by difference items in the previous column. If the convexity requirement of eq. (22) is satisfied, the second differences are positive.

Table B.1 Example of Difference Table (Valid)

k	$ln(m_k)$	$d1$	$d2$	$d3$	$d4$	$d5$
0	0	1	2	0	0	0
1	1	3	2	0	0	--
2	4	5	2	0	--	--
3	9	7	2	--	--	--
4	16	9	--	--	--	--
5	25	--	--	--	--	--

Table B.2 Example of Difference Table (Non-valid)

k	$ln(m_k)$	$d1$	$d2$	$d3$	$d4$	$d5$
0	0	1	2	-3	12	-30
1	1	3	-1	9	-18	--
2	4	2	8	-9	--	--
3	6	10	-1	--	--	--
4	16	9	--	--	--	--
5	25	--	--	--	--	--

Correction Procedure Part 1

In this part, correction algorithm aims to adjust the moments set so that they satisfy the necessary and sufficient condition given by eq. (21). It is an iteration method. In each step, the moments set are adjusted according to a certain principle and the iteration stops when eq. (21) is satisfied.

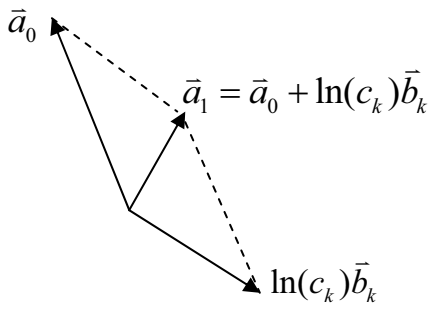

Fig. B.1 Variation of the vector of the third order differences due to moment correction.

The principle is given by follows.

If a moment m_k is changed as

$$(m_k)_1 = c_k (m_k)_0 \tag{B.1}$$

Its natural logarithm undergoes the following change

$$\ln(m_k)_1 = \ln c_k + \ln(m_k)_0 \tag{B.2}$$

Where $ln(m_k)_0$ is its initial value and $ln(m_k)_1$ its finial value. The consequent change in the third order differences vector (i.e. elements of column d2 of Table 1 and Table 2) is

$$\vec{a}_1 - \vec{a}_0 = (\ln c_k)\vec{b}_k \tag{B.3}$$

Where $\vec{a}_1$ and $\vec{a}_0$ are initial and final vectors of the third order differences respectively, while $\vec{b}_k$ is the response vector describing the change of the vector of third order differences to a unit increase in $ln(m_k)$. $\vec{a}_1$ represents a minimum length when it results orthogonal to $\vec{b}_k$, as shown in Fig. B.1. At this time, there is a relationship that

$$\left(\vec{a}_0 + \ln(c_k)\vec{b}_k\right)\cdot\vec{b}_k = 0 \tag{B.4}$$

The value of C_k through which $\vec{a}_1$ is minimized is thus obtained by

$$\ln(c_k) = -\cos(\vec{a}_0, \vec{b}_k)\frac{|\vec{a}_0|}{|\vec{b}_k|} = -\frac{(\vec{a}_0 \cdot \vec{b}_k)}{|\vec{b}_k|^2} \tag{B.5}$$

The resulting minimum squared amplitude is

$$|\vec{a}_1|^2 = |\vec{a}_0 + \ln(c_k)\vec{b}_k|^2 = |\vec{a}_0|^2\left[1 - \cos^2(\vec{a}_0, \vec{b}_k)\right] \tag{B.6}$$

The principle that correct moments set during each iteration step is to choose the index of moment which should achieves the maximum smoothness of the function $ln(m_k)$ after correction. The third order difference is taken as the indicator of smoothness. Thus the index k* of the moment that must be corrected is chosen as the one that gives the largest $\cos^2(\vec{a}_0, \vec{b}_k)$ for any moment of index k. The resulting correction term c_{k*} is

$$\ln(c_{k^*}) = -\cos(\vec{a}_0, \vec{b}_{k^*})\frac{|\vec{a}_0|}{|\vec{b}_{k^*}|} = -\frac{(\vec{a}_0 \cdot \vec{b}_{k^*})}{|\vec{b}_{k^*}|^2} \tag{B.7}$$

The original procedure search k* from k=0 to k=5. In the current implementation, k=0, and k=3 are skipped which means moment 0, and 3 are never adjusted.

The overall correction procedure for part 1 is shown in Fig. B.2

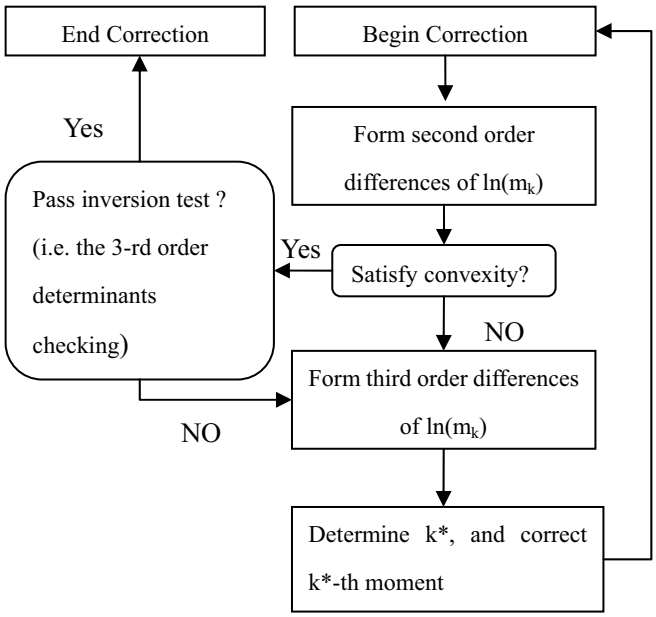

Fig. B.2 The overall correction procedure for part 1

Correction Procedure Part 2

Sometimes correction procedure described in part 1 fails after a certain number of iteration, such as 20 or 100. At this time, the moments set is forced to satisfy eq. (21) by directly set them to be the moments of the mean distribution of two log-normal distributions. A log-normal distribution has the following form:

$$n(L) = N_T \frac{\exp\left[\frac{-(\ln L - \mu)^2}{2\sigma^2}\right]}{L\sigma\sqrt{2\pi}} \tag{B.8}$$

Corresponding to the following generic moment m_k

$$m_k = N_T \exp\left(k\mu + \frac{k^2\sigma^2}{2}\right) \tag{B.9}$$

Where N_T is the total number of droplet, μ is the mean droplet radius (only approximately), and σ is the variance of the distribution. The three parameters for the first distribution are calculated by forcing only m_0, m_1, m_3 to be equal to those of the original set of moments, whereas the three parameters of the second distribution are calculated by forcing m_0, m_2, m_3.